Original Article

Anlotinib suppresses lung adenocarcinoma growth via inhibiting FASN-mediated lipid metabolism

Juan Shen[1,2#^], Jie Huang[2#^], Yu Huang[3], Yidan Chen[2], Jiawei Li[2], Peihua Luo[4], Qianyun Zhang[5], Yao Qiu[2], Lie Wang[6], Hong Jiang[7], Shenglin Ma[1,2,8], Xueqin Chen[1,2,8^]

[1]Department of Thoracic Oncology, Affiliated Hangzhou First People's Hospital, Zhejiang University School of Medicine, Hangzhou, China; [2]Department of Thoracic Oncology, Key Laboratory of Clinical Cancer Pharmacology and Toxicology Research of Zhejiang Province, Affiliated Hangzhou Cancer Hospital, Zhejiang University School of Medicine, Hangzhou, China; [3]Academy of Chinese Medical Sciences, Zhejiang Chinese Medical University, Hangzhou, China; [4]Center for Drug Safety Evaluation and Research of Zhejiang University, College of Pharmaceutical Sciences, Zhejiang University, Hangzhou, China; [5]Department of Oncology, Liyang People's Hospital, Liyang, China; [6]Institute of Immunology and Bone Marrow Transplantation Center, First Affiliated Hospital, Zhejiang University School of Medicine, Hangzhou, China; [7]Department of Thoracic Surgery, Affiliated Hangzhou First People's Hospital, Zhejiang University School of Medicine, Hangzhou, China; [8]Cancer Center, Zhejiang University, Hangzhou, China

Contributions: (I) Conception and design: S Ma, X Chen, J Shen; (II) Administrative support: P Luo, L Wang; (III) Provision of study materials or patients: H Jiang, X Chen, S Ma; (IV) Collection and assembly of data: J Shen, Y Huang, Q Zhang, J Li, Y Qiu; (V) Data analysis and interpretation: J Shen, J Huang, Y Chen; (VI) Manuscript writing: All authors; (VII) Final approval of manuscript: All authors.

[#]These authors have contributed equally to this work.

Correspondence to: Hong Jiang. Department of Thoracic Surgery, Affiliated Hangzhou First People's Hospital, Zhejiang University School of Medicine, Hangzhou 310006, China. Email: hh110120@126.com; Shenglin Ma. Department of Thoracic Oncology, Affiliated Hangzhou First People's Hospital, Zhejiang University School of Medicine, Hangzhou 310006, China. Email: mashenglin@medmail.com.cn; Xueqin Chen. Department of Thoracic Oncology, Affiliated Hangzhou First People's Hospital, Zhejiang University School of Medicine, Hangzhou 310006, China. Email: chenxueqin@zju.edu.cn.

Background: Anlotinib, a vascular endothelial growth factor receptor (VEGFR) inhibitor, has been widely used in advanced lung cancer patients, but the intrinsic mechanism of cancer cell elimination is not fully disclosed. In this study, we reported that anlotinib suppressed lung adenocarcinoma (LUAD) growth through inhibiting fatty acid synthase (FASN)-mediated lipid metabolism.

Methods: To investigate the underlying mechanisms of anlotinib, an A549 cell line-derived xenograft model was constructed and a proteomics technique was employed to screen potential markers. Gas chromatography-mass spectrometry (GC-MS) profiling of medium-long chain fatty acid and neutral lipid droplet fluorescence staining were employed to detect lipid metabolism in cancer cells. Subsequently, the effects of anlotinib on FASN expression were determined by reverse transcription-quantitative polymerase chain reaction (RT-qPCR) and western blot. Short hairpin RNA (shRNA) knockdown of FASN was used to assess the role of FASN in the antitumor effect of anlotinib. A patient-derived xenograft (PDX) model was established to validate the efficacy of anlotinib in the patient and IHC staining of FASN was examined.

Results: Our data revealed that anlotinib significantly decreased the expression of proteins related to lipid metabolism. GC-MS profiling of medium-long chain fatty acid and neutral lipid droplet fluorescence staining validated that anlotinib could disturb the fatty acid metabolism in cancer cells, especially de novo lipogenesis. Mechanically, the messenger RNA (mRNA) and protein of FASN were down-regulated by anlotinib in A549 cells and FASN knockdown could diminish the antitumor effect of anlotinib *in vitro*. Remarkable tumor shrinkage by anlotinib was further shown in a patient with multiple-line treatment failure, and FASN reduction was evidenced in the corresponding patient-derived xenograft (PDX) model.

^ ORCID: Juan Shen, 0000-0002-0377-6571; Jie Huang, 0000-0003-0381-1549; Xueqin Chen, 0000-0003-2299-6876.

Conclusions: Anlotinib could inhibit the growth of LUAD through FASN-mediated lipid metabolism. Our findings provide new insights into the antitumor mechanism of anlotinib in lung adenocarcinoma.

Keywords: Anlotinib; lipid metabolism; fatty acid synthase (FASN); lung adenocarcinoma

Submitted Oct 13, 2022. Accepted for publication Dec 02, 2022.
doi: 10.21037/atm-22-5438
View this article at: https://dx.doi.org/10.21037/atm-22-5438

Introduction

Lung cancer is the leading cause of global cancer-related deaths, and the majority of lung cancer cases are diagnosed at advanced stages (1). Anlotinib, as an anti-angiogenesis agent, has achieved high efficacy (2) and is approved for use in advanced lung cancer patients who have received at least 2 systemic chemotherapeutic regimes by the National Medical Products Administration (NMPA) in China. Anlotinib blocks the neoangiogenesis in tumors primarily through direct inhibition of vascular endothelial growth factor receptor (VEGFR), fibroblast growth factor receptor (FGFR), platelet-derived growth factor receptor (PDGFR) in endothelial cells (3,4), and exerts an indirect action on endothelial cells via decreasing the secretion of pro-angiogenesis factor chemokine (C-C motif) ligand 2 (CCL2) by tumor cells (5). Besides, anlotinib could also inhibit tumor cell proliferation directly, which was indicated in previous study (6). For instance, anlotinib could inhibit the growth of lung cancer stem cells via blocking the phosphorylation of nuclear factor kappa B (NF-κB) signaling cascade (7). Other researchers have demonstrated that anlotinib could induce apoptosis in pancreatic cancer cells through the accumulation of reactive oxygen species (ROS) (8). However, the direct anti-tumor effect mechanisms of anlotinib in lung adenocarcinoma (LUAD) are still largely unclear and remain to be further investigated.

Metabolic reprogramming, well recognized as a hallmark of cancer, vigorously participates in the proliferation of cancer cells as well as the tumor-promoting microenvironment (9). Liposome remodeling, as a metabolic feature of cancer cells, broadly includes alterations in fatty acid (FA) uptake, *de novo* lipogenesis, lipid droplet (LD) storage, and FA β-oxidation (10). Either *de novo* biosynthesis or exogenous uptake of FA has been widely shown to provide cancer cells with intensive fuel to maintain their proliferation through the β-oxidation of FA, even under nutrition stress (11), and to neutralize the oxidative stress triggered by multiple modalities such as radiation or chemotherapy through lipid oxidation (12,13). It has been observed that anlotinib significantly modulates the plasma metabolomics variation, such as aminoacyl-transfer RNA biosynthesis, alanine, aspartate, and glutamate metabolism, suggesting a close correlation between anlotinib treatment and metabolism (14). However, little is known about anlotinib-mediated metabolic reprogramming of tumors, especially in the context of lipid metabolism, in cancer cells themselves. Hence, we explored the relevance of cancer cell metabolism regulated by anlotinib.

In our study, in order to delineate the effective elimination mechanisms of anlotinib in LUAD cells, we investigated the regulation of the lipid metabolic profile induced by anlotinib in transplanted tumors with proteomics analysis techniques, which was further examined in A549 cells using metabolomics and lipid droplet fluorescence staining. We identified fatty acid synthase (FASN) as the key regulator in the anlotinib-induced lipid metabolism. This study sheds new light on the mechanism by which anlotinib eliminates lipid metabolism. We present

Highlight box

Key findings

- Anlotinib could directly target on LUAD cells through the reprogramming of fatty acid metabolism.

What is known and what is new?

- Anlotinib could block neoangiogenesis via attenuating the activation of VEGFR2 on endothelial cells in the LUAD microenvironment.
- Anlotinib could inhibit the growth of LUAD cells effectively both *in vivo* and *in vitro*, complemented with significant metabolic alterations. Inhibition of FASN-mediated lipid metabolism might be the key factor contributing to the antitumor-effect of anlotinib.

What is the implication, and what should change now?

- Our findings provide new insights into the antitumor mechanism of anlotinib in LUAD.

the following article in accordance with the ARRIVE and MDAR reporting checklists (available at https://atm.amegroups.com/article/view/10.21037/atm-22-5438/rc).

Methods

Cell culture

The human LUAD cell line A549 (RRID: CVCL_0023) was purchased from American Type Culture Collection (ATCC, Manassas, VA, USA) and cultured in Roswell Park Memorial Institute (RPMI) 1640 medium supplemented with 10% fetal bovine serum (FBS), 1% penicillin, and 1% streptomycin. Cells were cultivated at 37 ℃ in a humidified atmosphere containing 5% CO_2.

Chemotherapeutic agents

Anlotinib powder was kindly provided by Chiatai Tianqing (CTTQ) pharma (Jiangsu, China). Anlotinib was dissolved in dimethyl sulfoxide (DMSO), and stored at −80 ℃ in the dark. For all experimental timepoints, the final DMSO concentration was less than 0.1%. The half maximal inhibitory concentration (IC50) of anlotinib on A549 cells was tested to be about 3.05 μM at 48 h and about 2.35 μM at 72 h (data not shown), which generally agreed with the literature (6). Treatment concentrations were determined based on the experimentally determined IC50 value.

Animal Xenograft models

All animal experiments were carried out with approval by the Ethics Committee of Zhejiang Chinese Medical University Laboratory Animal Research Center (No. IACUC-20181210-01), in compliance with the Chinese guidelines for the care and use of animals. Animals were housed in specific-pathogen-free (SPF)-grade conditions under regular dark-light cycles during experiments. A protocol was prepared before the study without registration. For cell line-derived xenograft models, a suspension of 1×10^6 A549 cells was subcutaneously injected into the right flank of each 5–6-week-old male BLAB/c nude mouse and mice were then used for *in vivo* drug studies. For the patient-derived xenograft (PDX) model construction, a patient from Affiliated Hangzhou First People's Hospital, Zhejiang University School of Medicine with treatment failure from multiple modalities was enrolled in this study with signed written informed consent by the patient's legal guardian. The ethical approval was obtained from the Ethics Committee of Affiliated Hangzhou First People's Hospital, Zhejiang University School of Medicine (No. 2019007-01) and the study was conducted in accordance with the Declaration of Helsinki (as revised in 2013). Fresh tumor specimens (2 mm × 2 mm) were obtained by percutaneous intrapulmonary tumor puncture and transferred to the animal laboratory within 1 h in cryic-saline. A 5–6-week-old male anesthetized nonobese diabetic/severe combined immunodeficient (NOD/SCID) mouse was placed on a sterile, constant temperature operating table, the back skin was opened after shaving, and the incision was sutured after implantation of the specimen. After the surgery, we regularly observed the general status and tumor formation of the mouse. When the subcutaneous tumor had grown to the size of about 10 mm × 10 mm, it was collected and implanted in new mice for passaging. After 3 generations of successive inoculations had been performed, mice bearing the fourth generation xenografts were used for subsequent experiments.

In vivo drug studies

As the tumor size reached about 100 mm^3, tumor-bearing mice were randomized into a Control group and Anlotinib group (6 or 7 mice each), and administrated with normal saline or 1.5 mg/kg anlotinib by oral gavage daily for 2 weeks, respectively. Tumor width and length and mice body weight were measured 3 times a week and the tumor volumes were scored according to the following equation: Volume (mm^3) = width^2 (mm^2) × length (mm) $\times 2^{-1}$. Blind measurements were carried out to avoid unconscious biases. The mice were euthanized with carbon dioxide inhalation until the tumor volume reached 1,500 mm^2 or mice were at an early sign of distress. Tumors were surgically dissected and weighted, then half of the tumors were fast-frozen and the other half were made into formalin-fixed and paraffin-embedded (FFPE) slides for immunohistochemistry staining.

Proteomics profiling

Samples were sent to Oebiotech (Shanghai, China) for isobaric tags for relative and absolute quantification (iTRAQ)-based proteomic analysis. The following is a brief outline: extract the total protein from the sample using sodium dodecyl sulfate (SDS) lysate, take out a portion for protein concentration determination and sodium dodecyl sulfate-polyacrylamide gel electrophoresis (SDS-PAGE),

take out another portion for trypsin digestion and iTRAQ labeling (AB Sciex, Framingham, MA, USA), then take equal amounts of each labeled sample and mix the samples at a flow rate of 4 μL/min to a ChromXP C18 (3 μm, 150 Å) trap column, using Ekspert nanoLC 415 system (Sciex, Concord, ON, Canada) for chromatography separation, and then acquire tandem mass spectrometry (MS) data using information-dependent acquisition (IDA) mass spectrum techniques. Finally, the samples were analyzed by ProteinPilot software (v.5.0; Sciex) for detection and library search (Uniprot human/mmu protein database). The plausible proteins were screened according to the criteria of unused >1.3 and peptides (95%) ≥1; blank values were removed, and the differentially expressed proteins (DEPs) were screened according to the differential screening condition of foldchange =1.5. After the DEPs were obtained, they were subjected to Gene Ontology/Kyoto Encyclopedia of Genes and Genomes (GO/KEGG) enrichment analyses to characterize their functions.

RNA isolation and reverse transcription-quantitative polymerase chain reaction (RT-qPCR)

Total RNA was extracted with TRIzol reagent and a complementary DNA (cDNA) reverse transcription kit (R223-01; Vazyme, Nanjing, China) was used to prepare cDNA. Gene expression analysis was conducted using SYBR Green Supermix (Vazyme, R223-01) in CFX connect light cycler (CFX-Touch 96; Bio-Rad, Hercules, CA, USA), according to the manufacturer's instructions. A total of 1,000 ng RNA of each sample was subjected to RT-qPCR experiments and samples were tested in triplicate. The primer sequences are listed in Table S1.

Neutral lipid droplet fluorescence staining

BODIPY 493/503 (Shanghai Maokang Biotechnology, Shanghai, China) is a commonly-used agent for staining intracellular lipid droplets to monitor lipid storage (15,16). Briefly, the cells were seeded on coverslips and stained with BODIPY 493/503 at 2 μM final concentration for 15 min at 37 ℃ in the dark according to the manufacturer's instructions. Cells were then briefly washed with phosphate-buffered saline (PBS), fixed with 4% paraformaldehyde (PFA), stained with 4',6-diamidino-2-phenylindole (DAPI; Dojindo, Gaithersburg, MD, USA; D523) for 5 min at room temperature in the dark. The images were captured and analyzed by an Olympus FluoView 10i confocal microscope (Olympus, Tokyo, Japan).

Gas chromatography-mass spectrometry

We suspended 1×10^7 cells in 1 mL of methanol/chloroform and then sonicated them for 30 min. For methylation, 2 mL of 1% sulfuric acid-methanol solution was added to the supernatant at 80 ℃ for half an hour. A total of 1 mL of hexane was used for extraction and washed with 5 mL of pure water. Then, 500 μL of the supernatant was mixed with 25 μL of methyl nonadecanoate as an internal standard and then entered into gas chromatography-mass spectrometry (GC-MS) detection with a 10:1 split injection. The samples were separated on an Agilent DB-WAX capillary column (30 m length, 0.25 mm inner diameter, 0.25 μm phase thickness; Agilent, Santa Clara, CA, USA) with a gas chromatographic system. Quality control (QC) samples were set up at certain intervals to detect and evaluate the stability and reproducibility of the system. An Agilent 7890/5975C (Agilent, USA) was used for the MS analysis.

Protein isolation and western blot

Cells were lysed with lysis buffer containing 1% NP-40, 25 mM Tris HCl (PH 7.4), 150 mM NaCl, 1 mM ethylenediamine tetraacetic acid (EDTA), 5% glycerinum. Protein lysates were separated on 4–20% SDS-PAGE (Beyotime, P0056B) and transferred to polyvinylidene fluoride (PVDF) membranes. The cells were then incubated with primary and secondary antibodies and signal detection using enhanced chemiluminescence (ECL) plus reagents (Beyotime; P0018M). Quantitative image analysis was performed using Image J software (National Institutes of Health, Bethesda, MD, USA). Primary antibodies directed against β-actin (Bioker, Milan, Italy; BK7018) and FASN (Huabio, Woburn, MA, USA; R1706-8) were used. The secondary anti-rabbit IgG antibody (db10002) was purchased from Diagbio (Zhejiang, China).

Plasmid transfection

The pcDNA3.1-oeFASN (PPL00172-2a), pLKO.1-FASN-shRNA plasmids and vectors were purchased from the Public Protein/Plasmid Library (Jiangsu, China). The short hairpin RNA (shRNA) sequences were as follows: FASN-shRNA (5'-3'): AGAGCACCTTTGATGACAT; negative control (5'-3'): GTTCTCCGAACGTGTCACGTT. Cells (1×10^5) were seeded into 6-well plates and grown to

70–80% confluence. Transfection was performed using Polyjet™ Reagent (SignaGen, Frederick, MD, USA; SL100688) following the manufacturer's recommendations. Fresh complete medium was replaced at 12–18 h post transfection and cells were cultured for another 36 hours and then collected for further analysis.

Cell viability assay

A549 cells [1,500–2,000] were plated in a 96-well plate 24 h before treatment initiation. Indicated concentrations of anlotinib or 0.1% DMSO were added to complete medium for 24, 48, or 72 h. Cell viability was evaluated using cell counting kit-8 [MedChemExpress (MCE), Monmouth Junction, NJ, USA; HY-K0301] following the manufacturer's instructions. The absorbance at 450 nm was measured.

Colony formation assay

A total of 300 cells were seeded in each well of a 12-well plate, and anlotinib was administered following 24 h of adherence. Cells were incubated for 15 days until clones with more than 50 cells were generated. The clones were fixed, stained with 0.5% crystal violet for 30 min, photographed, and counted.

Immunohistochemistry

Formalin-fixed paraffin-embedded (FFPE) slices were baked in an oven at 60 ℃ for 2 h, deparaffinized twice in xylene, and washed twice in distilled water. The sections were placed in a beaker containing boiling repair solution, and the beaker was placed in an autoclave, heat treated for 2 min, and then cooled. The slices were dropwise with primary antibody and incubated overnight at 4 ℃ and continued for 1 h at 37 ℃ the next day. The secondary anti-mouse or anti-rabbit IgG antibody (ZSGB-BIO, DS-0004) was added dropwise after washing with PBS buffer and incubated for 25 min at 37 ℃. After washing with PBS, diaminobenzidine (DAB) was used for color development under microscopic observation. Primary antibodies include Ki67 (ZSGB-BIO, TA800648), cytokeratin (CK) (ZSGB-BIO, Beijing, China; ZM-0069), and FASN (Huabio, R1706-8). Immunoreactive score (IRS) (17) was evaluated and calculated by professional pathologists.

Statistical analyses

All data were performed in 3 independent experiments. Statistical analyses were performed using GraphPad Prism v.7.0 (GraphPad Software, San Diego, CA, USA). Student's *t*-test was used for comparison between two groups. Analysis of variance (ANOVA) was used to analyze differences between 3 or more groups. Statistically significant are represented as P-values <0.05.

Results

Anlotinib disturbed lipid metabolism of lung adenocarcinoma cells in vivo

To delineate the mechanisms by which anlotinib directly impacted on LUAD cells *in vivo*, we established mice xenografts derived from A549, a widely used human LUAD cell line. As shown in *Figure 1A*,*1B*, anlotinib could significantly dampen the tumor growth of A549 xenografts without obvious body weight loss (*Figure 1C*). Through NanoLC-ESI-MS/MS based proteomics profiling of the grown tumors matching with human protein database matching, we identified 1,290 downregulated proteins and 709 upregulated proteins which were obviously impacted with anlotinib administration (*Figure 1D* and https://cdn.amegroups.cn/static/public/atm-22-5438-1.xlsx). Interestingly, those down-regulated proteins were enriched in energy metabolism-related pathways (*Figure 1E*), including carbon metabolism, fatty acid metabolism, glycolysis/gluconeogenesis, fatty acid degradation, and so on. It has been increasingly shown that fatty acid metabolism is critical to cancer formation and therapy resistance. Therefore, we intended to disclose whether anlotinib could eliminate LUAD cells through modulating fatty acid metabolism. As illustrated in *Figure 1F*, all identified proteins associated with fatty acid metabolism remarkably decreased. Indeed, lipidomics confirmed an immense decrease of saturated fatty acid, polyunsaturated fatty acid, and monounsaturated fatty acid in the anlotinib group (*Figure 1G*, Table S2). Accordingly, we showed that the size and counts of lipid droplets significantly decreased in anlotinib-administrated A549 cells (*Figure 1H*). Thus, our data demonstrated that anlotinib reduced the fatty acid content in LUAD cells, and remodeled fatty acid metabolism intracellularly.

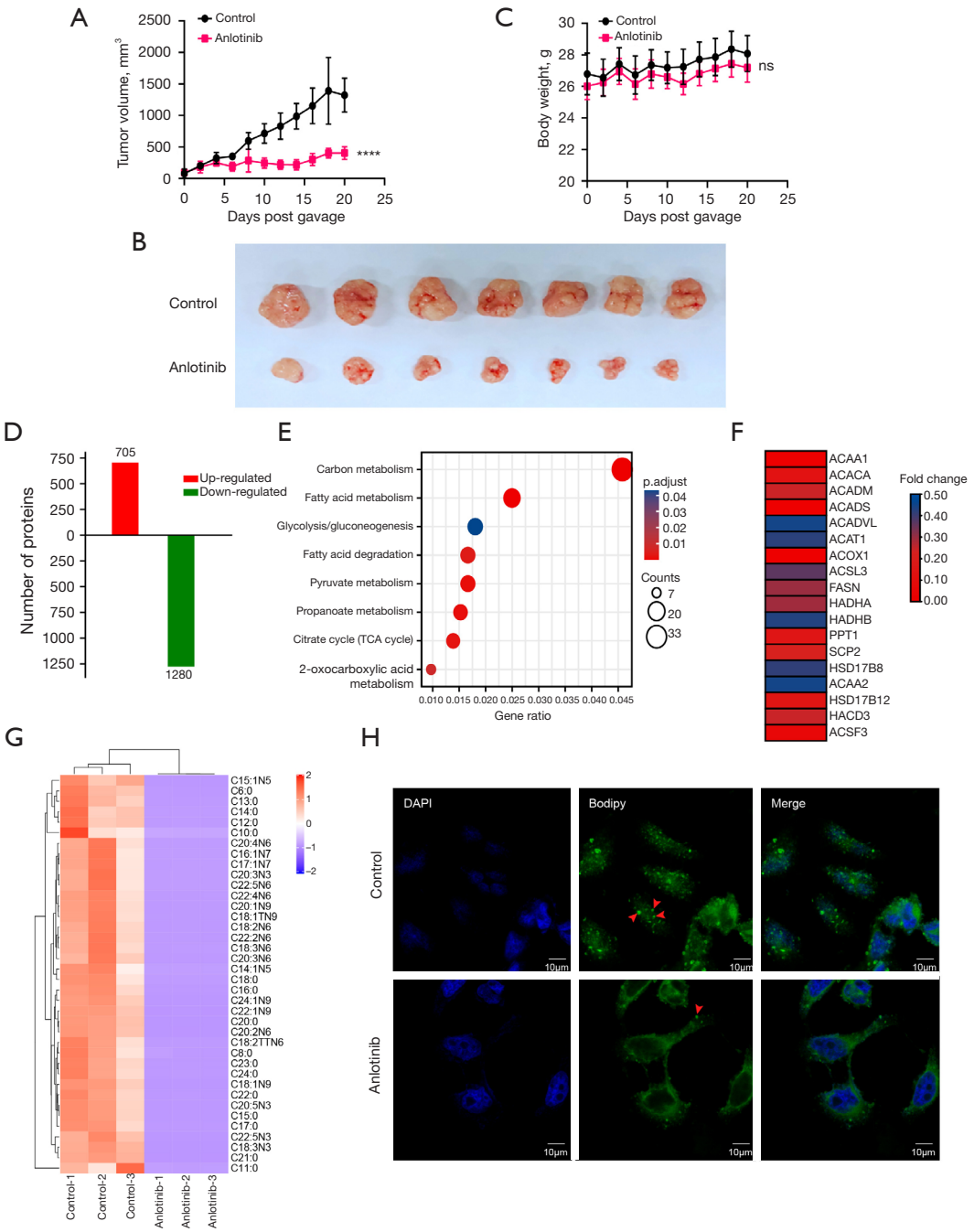

Figure 1 Anlotinib regulated lipid metabolism in A549 mice xenograft models. (A) The mass volumes of A549 subcutaneous xenografts in nude mice after treatment with placebo or anlotinib (0.8 mg/kg) (n=7 per group). (B) The picture of excited xenograft tumors from both control and anlotinib groups. (C) Body weights of mice in both groups are shown (n=7 per group). (D) Total counts of up-regulated/down-regulated proteins by anlotinib through proteomic profiling. (E) Metabolism-related pathways enrichment analyzed by KEGG analysis. (F) The visualization of the relative fold changes of lipid metabolism-related proteins between anlotinib group and placebo group by heatmap. (G) GC-MS analysis of medium and long chain fatty acids in A549 cells with indicated treatment for 72 h. (H) The neutral lipid droplet staining with Bodipy 493/503 in A549 cells with indicated treatment for 48 h (×120). Red arrowheads indicate neutral lipid droplets. Data are expressed as mean ± SEM. ****, P<0.0001; ns, not significant. KEGG, Kyoto Encyclopedia of Genes and Genomes; GC-MS, gas chromatography-mass spectrometry; SEM, standard error of the mean.

FASN was a key regulator in antitumor effect of anlotinib

We further examined the effect of anlotinib on those fatty acid metabolism-related factors, including FASN, sterol carrier protein 2 (SCP2), acetyl-CoA carboxylase alpha (ACACA), and acetyl-CoA acyltransferase 1 (ACAA1) in vitro; however, only FASN, the key enzyme in the *de novo* synthesis of fatty acids, was consistently reduced by anlotinib in the transcriptional levels, even at a relatively low dose (0.025 μM for 72 h) (*Figure 2A*). In addition, we investigated the potential clinical relevance between FASN expression and prognosis by searching The Cancer Proteome Atlas (TCPA) database. Importantly, high level of FASN was correlated with shorter progression free interval (log-rank P<0.001) (Figure S1). Next, western blotting assay validated the reduced expression of FASN at the protein level in A549 cells by anlotinib for 48 h (*Figure 2B*). To investigate the significance of FASN when anlotinib worked, we established A549-shFASN cells and A549-oeFASN cells with knockdown or ectopic expression of FASN (*Figure 2C*). The clonal formation assay showed that the clonogenic capacity of cells with low FASN expression significantly reduced, yet those with high FASN expression increased. Further, the antitumor effect of anlotinib decreased in FASN knockdown cells, yet over-expression of FASN could slightly enhance this inhibitory efficiency (*Figure 2D*). Additionally, the cell viability assay also demonstrated that FASN knockdown could significantly reduce the antitumor effect of anlotinib in A549 cells, yet A549-oeFASN cells remained sensitive to anlotinib (*Figure 2E*). Hence, we proposed that anlotinib inhibited A549 cells growth through FASN-regulated fatty acid metabolism.

Anlotinib elicited antitumor effects and decreased FASN expression in a PDX model

A 66-year-old Chinese woman with advanced LUAD experienced disease progression after multiple-line treatment (treatment history shown in *Figure 3A*) was administrated with 12 mg anlotinib per day from day 1 to 14 of every 21-day a cycle. After 2 cycles of anlotinib administration, the primary tumor shrunk to the minimum and the efficacy was assessed as partial response according to the response evaluation criteria in solid tumor (RECIST version 1.1) (18) (*Figure 3B-3E*). Anlotinib was well tolerated, and no serious side effects were observed until disease progression. The PDX models derived from this patient before anlotinib administration were constructed for drug screening. The primary tumor was successfully engrafted and passaged to the next mouse (*Figure 4A*). The initial xenograft, defined as F1, reached 500 mm^3 on day 120 post-inoculant, yet the average passage interval from F2 to F4 was only ~43 days (*Figure 4B*). Hematoxylin and eosin (H&E) and immunohistochemical (IHC) staining of CK and Ki-67 between the F4 xenograft and the parental tumor from the patient showed strong concordance (*Figure 4C*). Taken together, these results suggested that there was a consistency between F4 PDX xenografts and the original tumor from patient. Hence, F4 PDXs were employed for subsequent experiments. Compared with control mice, anlotinib could significantly suppress the tumor growth (P=0.0276, *Figure 4D*) and had no obvious impact on body weight (P=0.9482, *Figure 4E*). Notably, IHC staining validated that anlotinib significantly down-regulated the expression of FASN in the PDXs (P<0.0001, *Figure 4F*).

Discussion

Metabolism reprogramming has been widely accepted as a crucial factor facilitating tumor growth and metastasis either through enhancing the proliferation, survival, and migration abilities of cancer cells or training immune cells or stromal cells into tumor-promoting roles. Anlotinib, as an anti-angiogenesis agent, undoubtedly reconstitutes the metabolic microenvironment through blocking the nutrient supply. Here, however, our study provided the evidence that anlotinib could attenuate tumor growth through direct disturbance of lipid metabolism in LUAD cells.

It has been shown that anlotinib could inhibit glycolysis in myofibroblasts to reverse pulmonary fibrosis, which indicates that anlotinib might be capable of interfering with nutrition metabolism in cancer cells, thereby eliciting killing effects (19). A recent study also showed that anlotinib could interfere with amino acid metabolism in colon cancer cells leading to impaired protein synthesis and disruption of energy supply (20), which indicates that the killing effect of anlotinib in cancer cells is linked to metabolism. Surprisingly, their metabolomic results also showed that lipid metabolites were disturbed in the anlotinib group, and interestingly, our proteomic profiling of A549-derived xenografts demonstrated the extensive disturbance of tumor energy metabolism including fatty acid metabolism by anlotinib through human protein library matching. When we only looked at the mouse proteome

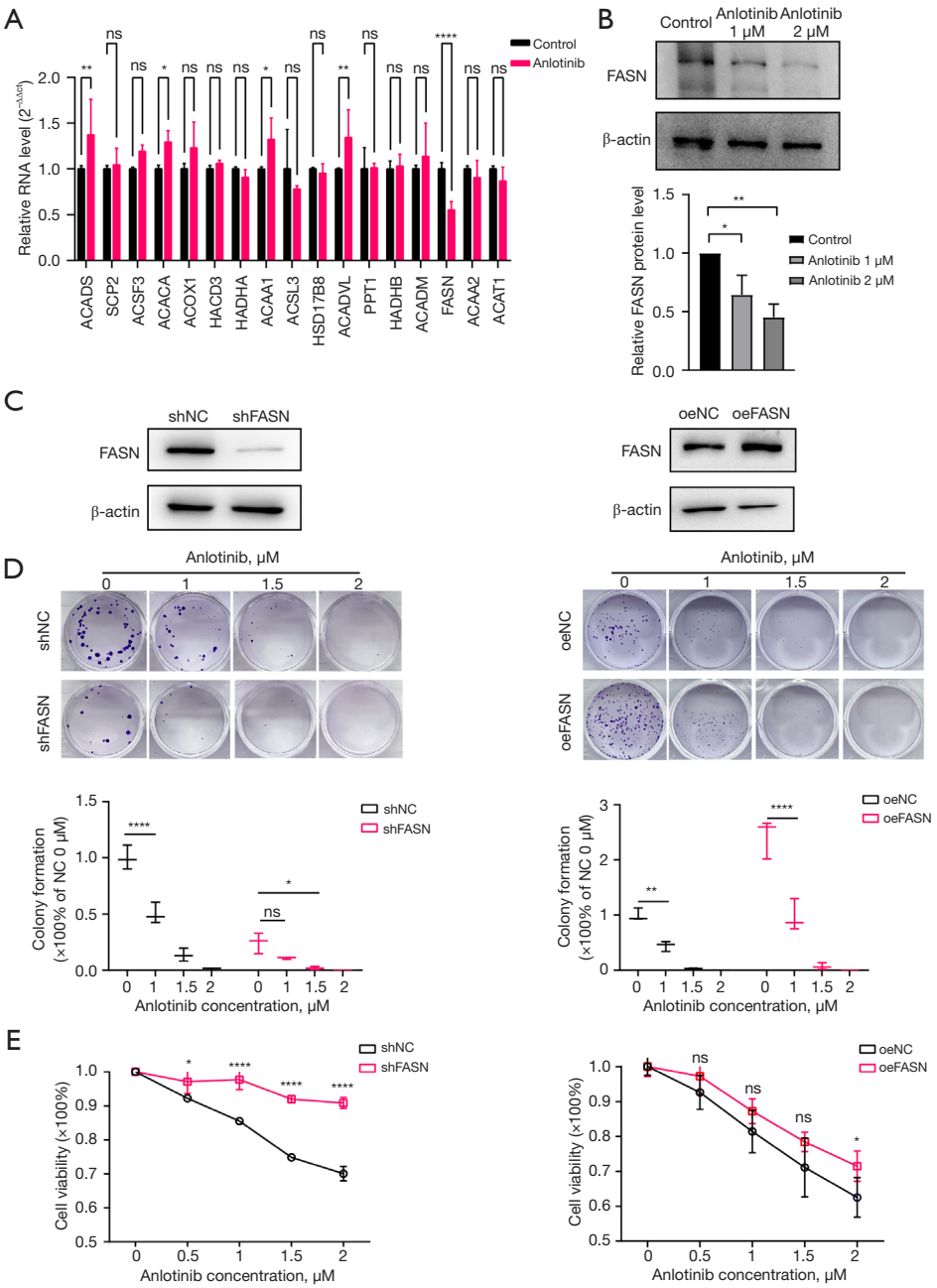

Figure 2 Anlotinib suppressed lung adenocarcinoma cells through FASN. (A) RT-qPCR analysis of lipid metabolism-related genes in A549 cells after indicated treatments for 72 h. (B) Upper panel: Western blotting analysis of FASN expression as anlotinib concentration increased. Lower Panel: the protein quantification results analyzed by ImageJ software. (C) FASN expression levels of A549-shFASN, A549-shNC, A549-oeNC, and A549-oeFASN cells as determined by western blot. (D) Upper panel: colony formation assay of A549-shFASN, A549-shNC, A549-oeNC, and A549-oeFASN cells treated with anlotinib at the indicated concentrations for 10 days. Lower panel: the colony formation rate, computed by calculating the ratio of clone numbers between indicated group and the untreated negative control (stained with 0.5% crystal violet for 30 min). (E) CCK-8 assay of A549-shFASN, A549-shNC, A549-oeNC, and A549-oeFASN cells treated with anlotinib at the indicated concentrations for 48 h. Data were expressed as mean ± SEM. *, P<0.05; **, P<0.01; ****, P<0.0001; ns, not significant. RT-qPCR, reverse transcription-quantitative polymerase chain reaction; FASN, fatty acid synthase; CCK-8, cell counting kit-8; SEM, standard error of the mean.

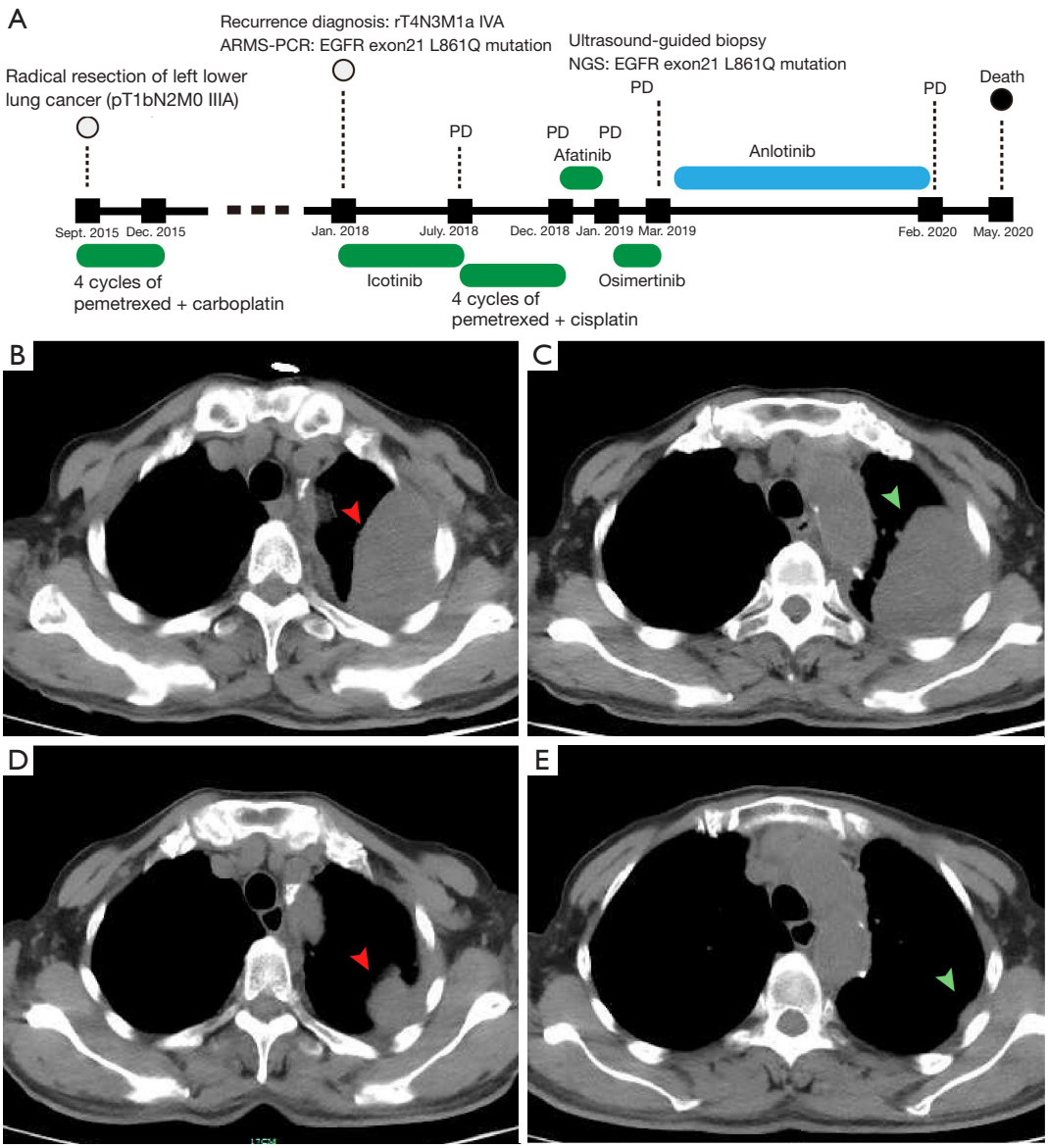

Figure 3 Anlotinib exhibited promising antitumor effects in an advanced lung adenocarcinoma patient with multiple treatment failure. (A) The timeline for entire treatment. Staging was performed as per AJCC 7th edition guideline. (B,C) CT images at baseline ahead of anlotinib treatment. (D,E) CT images at best response. Arrowheads with a same color indicate a same target lesion. AJCC, American Joint Committee on Cancer; CT, computed tomography; ARMS-PCR, amplification refractory mutation system polymerase chain reaction; EGFR, epidermal growth factor receptor; PD, progressive disease; NGS, next-generation sequencing.

(Table S3), the altered proteins were not significantly enriched in metabolism-related pathways, to some extent, which suggested that cancer cells might be the main cause of reshaped metabolic microenvironment by anlotinib.

FASN is a key protease in the end-stage of *de novo* lipogenesis, formerly known as oncogenic antigen-519 (21), and catalyzes the synthesis of saturated fatty acid palmitate in a dimeric functional form (22). Of interest, FASN is an emerging therapeutic target that has been extensively and intensively studied. FASN is found to be highly expressed in malignant tissues (22) including lung (23), breast (24), and colorectal (25) cancer. Furthermore, its over-expression is significantly associated with the detrimental prognosis and acquired drug resistance (25,26). Endogenous *de novo*

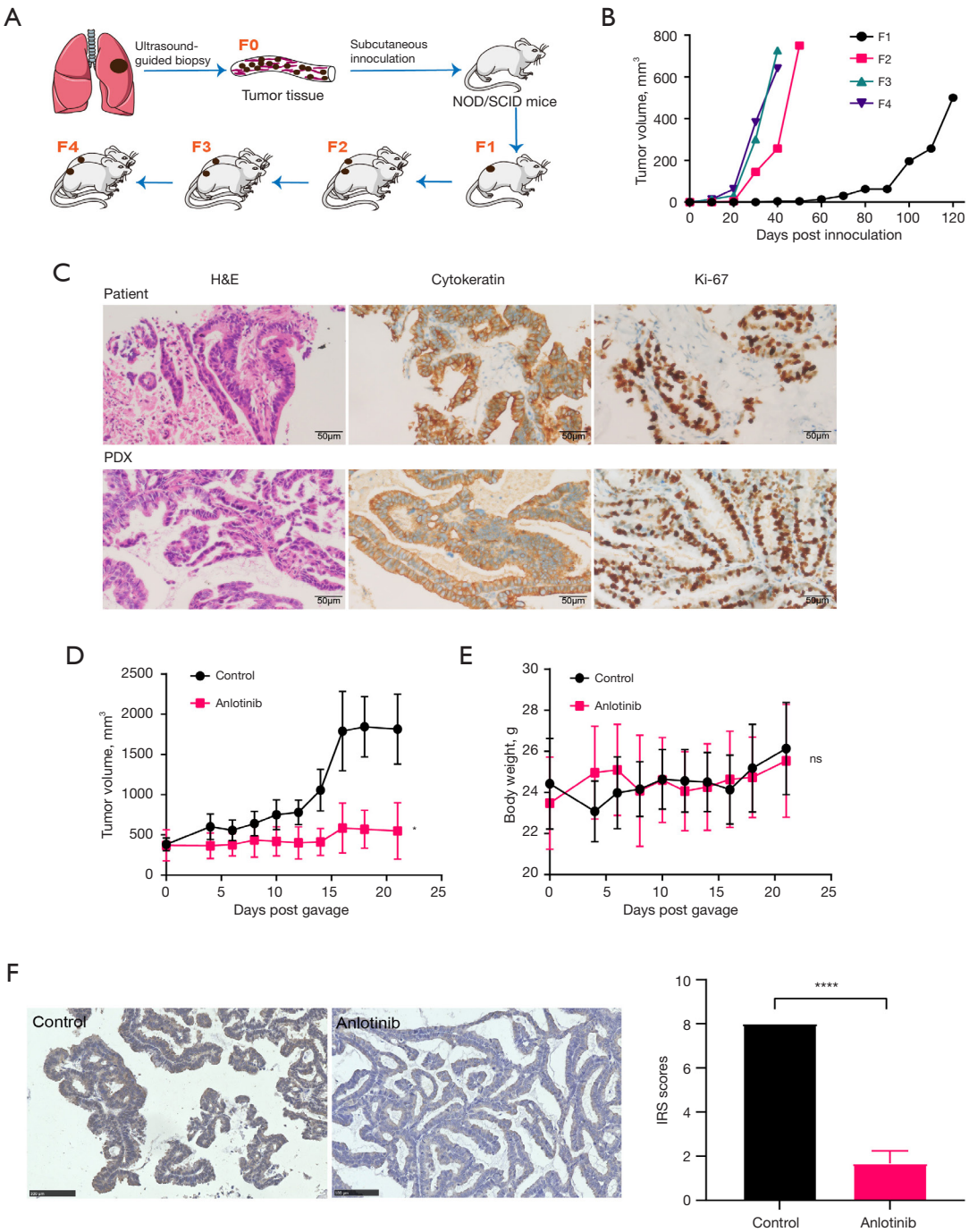

Figure 4 Anlotinib elicited robust antitumor effects and decreased FASN expression in a PDX model. (A) Schematic model presenting the procedure to construct the PDX model. (B) The tumor volume changes of PDX model iterations F1-F4 post inoculation. (C) H&E and IHC pictures of tumors from the established F4 PDX model and the parental tissue from the patient (×200). (D,E) The tumor volumes (D) and body weights (E) of PDX model mice treated with control or anlotinib (n=5 per group). (F) IHC staining of FASN in PDX models with or without treatment of anlotinib. Left panel shows the representative pictures, and panel is the calculated IRS. Data are expressed as mean ± SEM. *, P<0.05; ****, P<0.0001; ns, not significant as compared with the control group. NOD/SCID, anesthetized nonobese diabetic/severe combined immunodeficient; FASN, fatty acid synthase; PDX, patient-derived xenograft; IHC, immunohistochemical; IRS, immunoreactive score; H&E, hematoxylin and eosin staining; SEM, standard error of the mean.

synthesis, rather than exogenous uptake, is the primary fatty acid acquisition pathway for most cultured cancer cells in the presence of oxygen and abundant extracellular nutrients (27,28). Due to the high expression of FASN in tumors and the low demand for endogenous lipid synthesis in normal cells, FASN is considered a strong potential therapeutic target in various cancer types (22). In our study, FASN knockdown could reduce the antitumor activities of anlotinib, and A549 cells that ectopically expressed FASN with high proliferation capacity remained sensitive to anlotinib. Therefore, FASN may be a therapeutic target of anlotinib.

The lipid metabolism pathway most frequently involved in cancer is the phosphoinositide 3-kinase/protein kinase B (PI3K/AKT) signaling pathway (29,30), which is shown to be the main signal pathway triggering FASN expression. Receptor tyrosine kinases (RTKs) are major upstream regulators of PI3K/AKT signaling (31). Anlotinib is known to inhibit multiple RTKs including VEGFR, FGFR, and PDGFR (3), as well as some unconventional pharmacological targets such as GINS1 (32), MET (33), and EGFR (34). Studies are available on anlotinib blockade of the PI3K/AKT which is activated by VEGFR (35) or others (36,37). From the above iterative derivation, we speculate that anlotinib works by inhibiting the phosphorylation of RTK protein on the cell membrane, which in turn leads to the disruption of intracellular signaling pathways and ultimately hinders the expression of FASN. Previous paper has demonstrated that VEGFR2 expression was relatively low and difficult to obtain in A549 cells (38), which hints that anlotinib might kill lung cancer cells through other pathways instead of inhibiting VEGFR2 as in the endothelial cells. As a limitation, the underlying mechanism was not investigated in this research.

Due to the increasing emphasis on metabolic reorganization in tumors, therapeutic options targeting metabolism are considered to have high potential for transformative therapies. In recent years, FASN inhibitors have emerged in the area of cancer research (22,39,40); however, few of them have been approved as antineoplastic drugs because of their severe side effects. Anlotinib, as a well-tolerated drug, was firstly demonstrated to be capable of inhibiting FASN in LUAD. Intriguingly, it was recently reported that knockdown of FASN also could trigger an anti-angiogenic effect by post-translational modification of mammalian target of rapamycin (mTOR) (41), which implicates that FASN might be an alternative target in the anti-angiogenic effect of anlotinib.

Conclusions

In conclusion, we discovered that anlotinib could inhibit the growth of LUAD through FASN-mediated lipid metabolism. Our findings provide new insights into the antitumor mechanism of anlotinib in LUAD.

Acknowledgments

Funding: This research was funded by the Natural Science Foundation of Zhejiang Province (No. LY21H310002); Zhejiang Public Welfare Technology Application Research Project (No. LGF21H160021); and Science and Technology Development Project of Hangzhou (No. 202204A08).

Footnote

Reporting Checklist: The authors have completed the ARRIVE and MDAR reporting checklists. Available at https://atm.amegroups.com/article/view/10.21037/atm-22-5438/rc

Data Sharing Statement: Available at https://atm.amegroups.com/article/view/10.21037/atm-22-5438/dss

Conflicts of Interest: All authors have completed the ICMJE uniform disclosure form (available at https://atm.amegroups.com/article/view/10.21037/atm-22-5438/coif). The authors have no conflicts of interest to declare.

Ethical Statement: The authors are accountable for all aspects of the work in ensuring that questions related to the accuracy or integrity of any part of the work are appropriately investigated and resolved. Animal experiments were performed under a project license (No. IACUC-20181210-01) granted by the Ethics Committee of Zhejiang Chinese Medical University Laboratory Animal Research Center, in compliance with the Chinese guidelines for the care and use of animals. For the patient experiment, the study was conducted in accordance with the Declaration of Helsinki (as revised in 2013), and approved by the Ethics Committee of Affiliated Hangzhou First People's Hospital, Zhejiang University School of Medicine (No. 2019007-01). Written informed consent was provided by the patient's legal guardian.

References

1. Sung H, Ferlay J, Siegel RL, et al. Global Cancer Statistics 2020: GLOBOCAN Estimates of Incidence and Mortality Worldwide for 36 Cancers in 185 Countries. CA Cancer J Clin 2021;71:209-49.
2. Han B, Li K, Wang Q, et al. Effect of Anlotinib as a Third-Line or Further Treatment on Overall Survival of Patients With Advanced Non-Small Cell Lung Cancer: The ALTER 0303 Phase 3 Randomized Clinical Trial. JAMA Oncol 2018;4:1569-75.
3. Shen G, Zheng F, Ren D, et al. Anlotinib: a novel multi-targeting tyrosine kinase inhibitor in clinical development. J Hematol Oncol 2018;11:120.
4. Du Z, Lovly CM. Mechanisms of receptor tyrosine kinase activation in cancer. Mol Cancer 2018;17:58.
5. Lu J, Zhong H, Chu T, et al. Role of anlotinib-induced CCL2 decrease in anti-angiogenesis and response prediction for nonsmall cell lung cancer therapy. Eur Respir J 2019;53:1801562.
6. Xie C, Wan X, Quan H, et al. Preclinical characterization of anlotinib, a highly potent and selective vascular endothelial growth factor receptor-2 inhibitor. Cancer Sci 2018;109:1207-19.
7. Li Z, Tian J, Du L, et al. Anlotinib exerts anti-cancer efficiency on lung cancer stem cells in vitro and in vivo through reducing NF-κB activity. J Cell Mol Med 2021;25:5547-59.
8. Yang L, Zhou X, Sun J, et al. Reactive oxygen species mediate anlotinib-induced apoptosis via activation of endoplasmic reticulum stress in pancreatic cancer. Cell Death Dis 2020;11:766.
9. Hanahan D, Weinberg RA. Hallmarks of cancer: the next generation. Cell 2011;144:646-74.
10. Koundouros N, Poulogiannis G. Reprogramming of fatty acid metabolism in cancer. Br J Cancer 2020;122:4-22.
11. Röhrig F, Schulze A. The multifaceted roles of fatty acid synthesis in cancer. Nat Rev Cancer 2016;16:732-49.
12. Viswanathan VS, Ryan MJ, Dhruv HD, et al. Dependency of a therapy-resistant state of cancer cells on a lipid peroxidase pathway. Nature 2017;547:453-7.
13. Wang T, Fahrmann JF, Lee H, et al. JAK/STAT3-Regulated Fatty Acid β-Oxidation Is Critical for Breast Cancer Stem Cell Self-Renewal and Chemoresistance. Cell Metab 2018;27:136-150.e5.
14. Hu T, An Z, Sun Y, et al. Longitudinal Pharmacometabonomics for Predicting Malignant Tumor Patient Responses to Anlotinib Therapy: Phenotype, Efficacy, and Toxicity. Front Oncol 2020;10:548300.
15. Kuo A, Lee MY, Sessa WC. Lipid Droplet Biogenesis and Function in the Endothelium. Circ Res 2017;120:1289-97.
16. Qiu B, Simon MC. BODIPY 493/503 Staining of Neutral Lipid Droplets for Microscopy and Quantification by Flow Cytometry. Bio Protoc 2016;6:e1912.
17. Skoog L, Humla S, Isaksson S, et al. Immunocytochemical analysis of receptors for estrogen and progesterone in fine-needle aspirates from human breast carcinomas. Diagn Cytopathol 1990;6:95-8.
18. Eisenhauer EA, Therasse P, Bogaerts J, et al. New response evaluation criteria in solid tumours: revised RECIST guideline (version 1.1). Eur J Cancer 2009;45:228-47.
19. Chen W, Zhang J, Zhong W, et al. Anlotinib Inhibits PFKFB3-Driven Glycolysis in Myofibroblasts to Reverse Pulmonary Fibrosis. Front Pharmacol 2021;12:744826.
20. Jia Z, Zhang Z, Tian Q, et al. Integration of transcriptomics and metabolomics reveals anlotinib-induced cytotoxicity in colon cancer cells. Gene 2021;786:145625.
21. Kuhajda FP, Jenner K, Wood FD, et al. Fatty acid synthesis: a potential selective target for antineoplastic therapy. Proc Natl Acad Sci U S A 1994;91:6379-83.
22. Fhu CW, Ali A. Fatty Acid Synthase: An Emerging Target in Cancer. Molecules 2020;25:3935.
23. Gouw AM, Eberlin LS, Margulis K, et al. Oncogene KRAS activates fatty acid synthase, resulting in specific ERK and lipid signatures associated with lung adenocarcinoma. Proc Natl Acad Sci U S A 2017;114:4300-5.
24. Cairns J, Ingle JN, Kalari KR, et al. Anastrozole Regulates Fatty Acid Synthase in Breast Cancer. Mol Cancer Ther 2022;21:206-16.
25. Ecker J, Benedetti E, Kindt ASD, et al. The Colorectal Cancer Lipidome: Identification of a Robust Tumor-Specific Lipid Species Signature. Gastroenterology 2021;161:910-923.e19.
26. Tadros S, Shukla SK, King RJ, et al. De Novo Lipid Synthesis Facilitates Gemcitabine Resistance through Endoplasmic Reticulum Stress in Pancreatic Cancer. Cancer Res 2017;77:5503-17.

27. Boroughs LK, DeBerardinis RJ. Metabolic pathways promoting cancer cell survival and growth. Nat Cell Biol 2015;17:351-9.
28. Swinnen JV, Brusselmans K, Verhoeven G. Increased lipogenesis in cancer cells: new players, novel targets. Curr Opin Clin Nutr Metab Care 2006;9:358-65.
29. Ricoult SJ, Yecies JL, Ben-Sahra I, et al. Oncogenic PI3K and K-Ras stimulate de novo lipid synthesis through mTORC1 and SREBP. Oncogene 2016;35:1250-60.
30. Yi J, Zhu J, Wu J, et al. Oncogenic activation of PI3K-AKT-mTOR signaling suppresses ferroptosis via SREBP-mediated lipogenesis. Proc Natl Acad Sci U S A 2020;117:31189-97.
31. Haddadi N, Lin Y, Travis G, et al. PTEN/PTENP1: 'Regulating the regulator of RTK-dependent PI3K/Akt signalling', new targets for cancer therapy. Mol Cancer 2018;17:37.
32. Tang L, Yu W, Wang Y, et al. Anlotinib inhibits synovial sarcoma by targeting GINS1: a novel downstream target oncogene in progression of synovial sarcoma. Clin Transl Oncol 2019;21:1624-33.
33. Wang G, Sun M, Jiang Y, et al. Anlotinib, a novel small molecular tyrosine kinase inhibitor, suppresses growth and metastasis via dual blockade of VEGFR2 and MET in osteosarcoma. Int J Cancer 2019;145:979-93.
34. Liang J, Jin Z, Kuang J, et al. The role of anlotinib-mediated EGFR blockade in a positive feedback loop of CXCL11-EGF-EGFR signalling in anaplastic thyroid cancer angiogenesis. Br J Cancer 2021;125:390-401.
35. Song F, Hu B, Cheng JW, et al. Anlotinib suppresses tumor progression via blocking the VEGFR2/PI3K/AKT cascade in intrahepatic cholangiocarcinoma. Cell Death Dis 2020;11:573.
36. Lan W, Zhao J, Chen W, et al. Anlotinib Overcomes Multiple Drug Resistant Colorectal Cancer Cells via Inactivating PI3K/AKT Pathway. Anticancer Agents Med Chem 2021;21:1987-95.
37. Lu Y, Lin J, Duan M, et al. Anlotinib Suppresses Oral Squamous Cell Carcinoma Growth and Metastasis by Targeting the RAS Protein to Inhibit the PI3K/Akt Signalling Pathway. Anal Cell Pathol (Amst) 2021;2021:5228713.
38. Riquelme E, Suraokar M, Behrens C, et al. VEGF/VEGFR-2 upregulates EZH2 expression in lung adenocarcinoma cells and EZH2 depletion enhances the response to platinum-based and VEGFR-2-targeted therapy. Clin Cancer Res 2014;20:3849-61.
39. Liu Y, Gao GF, Minna JD, et al. Loss of wild type KRAS in KRASMUT lung adenocarcinoma is associated with cancer mortality and confers sensitivity to FASN inhibitors. Lung Cancer 2021;153:73-80.
40. Qu H, Shan K, Tang C, et al. A novel small-molecule fatty acid synthase inhibitor with antitumor activity by cell cycle arrest and cell division inhibition. Eur J Med Chem 2021;219:113407.
41. Bruning U, Morales-Rodriguez F, Kalucka J, et al. Impairment of Angiogenesis by Fatty Acid Synthase Inhibition Involves mTOR Malonylation. Cell Metab 2018;28:866-880.e15.

(English Language Editor: J. Jones)

Cite this article as: Shen J, Huang J, Huang Y, Chen Y, Li J, Luo P, Zhang Q, Qiu Y, Wang L, Jiang H, Ma S, Chen X. Anlotinib suppresses lung adenocarcinoma growth via inhibiting FASN-mediated lipid metabolism. Ann Transl Med 2022;10(24):1337. doi: 10.21037/atm-22-5438

Supplementary

Table S1 The primer sequences

Symbol	Forward primer	Reverse primer
FASN	CCATCTACAACATCGACACCAG	CTTCCACACTATGCTCAGGTAG
ACACA	TACCTTCTTCTACTGGCGGCTGAG	GCCTTCACTGTTCCTTCCACTTCC
HADHA	CTGTGTTTGAGGACCTTAGTCT	GTCTTTGGAAGTTTTCTCGGTC
PPT1	GGTGGAGAAGAAAATACCTGGA	CTGACACACTGTTGTTACTTGG
ACADS	CAGTTACACACCATCTACCAGT	GCTGGGAAGAGATGTTCCTTAT
ACOX1	CACAAGTAAACCAGCGTGTAAA	GTTCTTAGCCCACTCAAACAAG
ACAA1	TGGAAATATTACTTCGCGCTTG	AGCCACATTCTCAGAGGTTATC
SCP2	GGAGCTGAGAATTCAAGAGACT	AGTCACCAAAAACATAGCCAAC
HACD3	GATGTATTTCTGCCAGATGCTG	TTGTTCTGCATTTCTTCCATGG
ACSL3	CGTGTCTTCAAAACCATCTACC	TCTTGTCTTGACTCGGAGAAAA
HADHB	TTTCCATAAGACCTCTGAGCTG	TCATGTGGCATCAGGTCTTTAT
ACAA2	GCTCTCACGATTAATAGGCTCT	ACATTTCTGACACAGTAGGGAG
ACADVL	CCCGCCAAGAATGACGCTCTG	GCCCACGATCTCCACCAAACG
HSD17B8	ACTCTGTCCTCCCAGGGTTCATTG	GCGACCACATCTGCCACATCC
ACADM	GCCAGAGAGGAAATCATCCCAGTG	CCAAGTCCAAGACCTCCACAGTTC
ACSF3	CCAGGATTTCTTGCGTGCAGTTTG	GCCCGTGATGTTCTTCCACTTCTC
ACAT1	GCTCCTGTATATGCTGCATCTA	TGTTTGCTAGTACAACCAGACT
ACTB	CATGTACGTTGCTATCCAGGC	CTCCTTAATGTCACGCACGAT

https://dx.doi.org/10.21037/atm-22-5438

Table S2 Lipidomics analysis

Name	Fatty acids	Unit	Fold change	P-value	Anlo-1	Anlo-2	Anlo-3	Control-1	Control-2	Control-3
C21:0	Methyl heneicosanoate	μg/10^7	0.013272	1.02E-05	0.00183	0.001633	0.001571	0.134917	0.12483	0.119546
C18:3N3	Methyl linolenate	μg/10^7	0.006358	3.93E-05	0.003773	0.003391	0.003103	0.590954	0.52371	0.500263
C20:0	Methyl arachidate	μg/10^7	0.007866	0.000128	0.016951	0.015877	0.014418	2.103415	2.17001	1.732654
C20:2N6	cis-11,14-Eicosadienoic acid methyl ester	μg/10^7	0.01011	0.000189	0.037276	0.033379	0.031617	3.546054	3.69547	2.87465
C22:1N9	Methyl erucate	μg/10^7	0.010498	0.00024	0.032145	0.030801	0.02844	3.128542	3.13672	2.440216
C22:5N3	Methyl docosapentaenoate	μg/10^7	0.011894	0.000418	0.238373	0.23119	0.205216	22.16829	18.29826	16.26522
C15:1N5	Methyl cis-10-pentadecenoate	μg/10^7	0.010865	0.000578	0.005859	0.006139	0.006266	0.461593	0.654838	0.564582
C24:1N9	Methyl cis-15-tetracosenoate	μg/10^7	0.010606	0.000609	0.077901	0.071406	0.066535	7.642505	7.279086	5.429239
C18:1N9	Methyl oleate	μg/10^7	0.009058	0.000649	1.268814	1.240426	1.108427	144.1491	149.3471	105.9111
C15:0	Methyl pentadecanoate	μg/10^7	0.010541	0.0012	0.025363	0.025404	0.023501	2.538523	2.715308	1.791688
C20:5N3	cis-5,8,11,14,17-Eicosapentaenoic acid methyl ester	μg/10^7	0.009124	0.001216	0.099781	0.08876	0.084975	10.81182	11.55493	7.609683
C6:0	Methyl hexanoate	μg/10^7	0.005797	0.001337	3.32E-05	2.53E-05	4.35E-05	0.005339	0.007308	0.004946
C22:0	Methyl behenate	μg/10^7	0.008722	0.001622	0.004813	0.004163	0.003925	0.523495	0.586252	0.369322
C16:0	Methyl palmitate	μg/10^7	0.008801	0.001738	2.319649	2.2645	2.027522	291.7051	275.0945	184.436
C20:3N6	cis-8,11,14-Eicosatrienoic acid methyl ester	μg/10^7	0.007206	0.001783	0.057485	0.051038	0.047614	9.089898	6.741428	5.836345
C17:0	Methyl heptadecanoate	μg/10^7	0.011837	0.001909	0.028852	0.02756	0.024696	2.563282	2.625303	1.663527
C23:0	Methyl tricosanoate	μg/10^7	0.014419	0.001955	0.001067	0.00091	0.000979	0.07049	0.083341	0.051221
C18:2N6	Methyl linoleate	μg/10^7	0.010928	0.00246	0.372584	0.339095	0.317124	39.28767	31.41328	23.44665
C13:0	Methyl tridecanoate	μg/10^7	0.011211	0.002492	0.000268	0.000304	0.000217	0.022058	0.02994	0.018314
C24:0	Methyl tetracosanoate	μg/10^7	0.01096	0.002603	0.008365	0.007695	0.007319	0.739503	0.877321	0.516288
C22:2N6	cis-13,16-Docosadienoic acid methyl ester	μg/10^7	0.012537	0.002711	0.00987	0.007862	0.008618	0.889772	0.683405	0.528588
C20:1N9	cis-11-Eicosenoic acid methyl ester	μg/10^7	0.011047	0.002788	0.119863	0.112642	0.105008	12.48564	10.79091	7.274951
C18:2TTN6	Methyl linolelaidate	μg/10^7	0.004162	0.003124	0.029057	0.027552	0.023623	6.843269	7.919646	4.513267
C12:0	Methyl dodecanoate	μg/10^7	0.010604	0.003271	0.002159	0.001818	0.001589	0.143519	0.229848	0.15153
C22:4N6	Methyl docosatetraenoate	μg/10^7	0.015871	0.003314	0.054385	0.055919	0.047105	4.055834	3.553755	2.308522
C18:1TN9	Methyl elaidate	μg/10^7	0.00998	0.003378	3.162416	3.049903	2.806728	375.1158	317.0366	211.5903
C18:3N6	Methyl γ-linolenate	μg/10^7	0.008169	0.003575	0.001372	0.001292	0.001114	0.198304	0.1522	0.112046
C18:0	Methyl stearate	μg/10^7	0.010323	0.004111	1.104967	0.995756	0.881745	114.0606	110.7646	64.09216
C8:0	Methyl octanoate	μg/10^7	0.019009	0.004233	3.23E-05	2.44E-05	0.000104	0.003022	0.003521	0.001924
C20:4N6	Methyl arachidonate	μg/10^7	0.009998	0.004304	0.582484	0.530831	0.487059	68.53994	54.31482	37.21525
C14:0	Methyl myristate	μg/10^7	0.010251	0.004349	0.133369	0.128403	0.105959	9.502667	15.99569	10.37475
C17:1N7	Methyl cis-10-heptadecenoate	μg/10^7	0.00956	0.005823	0.080126	0.077949	0.066895	10.17525	8.166716	5.190935
C16:1N7	Methyl palmitoleate	μg/10^7	0.008701	0.006257	0.507634	0.50775	0.448202	73.16489	58.28312	36.75849
C20:3N3	cis-11,14,17-Eicosatrienoic acid methyl ester	μg/10^7	0.009961	0.006346	0.00691	0.006332	0.006317	0.867651	0.656732	0.439181
C22:5N6	Methyl docosapentaenoate	μg/10^7	0.00915	0.006487	0.004523	0.003945	0.003844	0.594033	0.453138	0.298442
C14:1N5	Methyl myristoleate	μg/10^7	0.009605	0.007908	0.0017	0.001587	0.001404	0.202296	0.18827	0.097803
C11:0	Methyl undecanoate	μg/10^7	0.010467	0.00856	1.35E-05	2.24E-05	4.1E-05	0.001646	0.002326	0.003376
C10:0	Methyl decanoate	μg/10^7	0.006603	0.03394	3.7E-05	3.1E-05	6.84E-05	0.004992	0.011189	0.004467
C4:0	Methyl butyrate	μg/10^7								
C22:6N3	cis-4,7,10,13,16,19-Docosahexaenoic acid methyl ester	μg/10^7								
Total_SFA	/	μg/10^7	0.00928	0.002038	3.647767	3.474127	3.093699	424.1226	411.3213	265.3317
Total_MUFA	/	μg/10^7	0.009631	0.002344	5.256459	5.098602	4.637905	626.5257	554.8834	375.2577
Total_PUFA	/	μg/10^7	0.010127	0.002068	1.497874	1.380585	1.26733	167.4835	139.9608	101.9481
Total_N3	/	μg/10^7	0.010834	0.000454	0.348838	0.329673	0.299612	34.43871	31.03364	24.81435
Total_N6	/	μg/10^7	0.009927	0.002883	1.149036	1.050912	0.967719	133.0448	108.9271	77.13376

https://dx.doi.org/10.21037/atm-22-5438

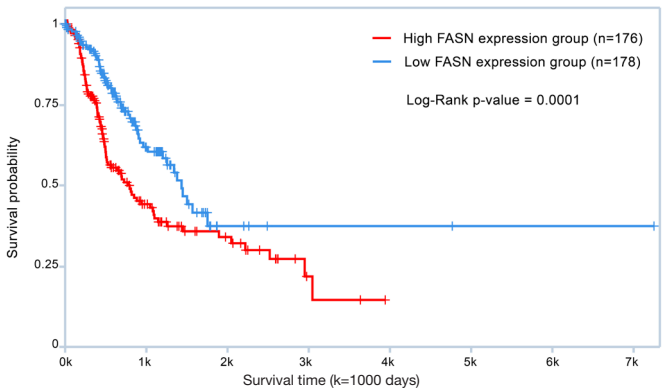

Figure S1 The association between FASN expression and progression free interval in lung adenocarcinoma patients using the TCPA database. Log-Rank test was used. FASN, fatty acid synthase; TCPA, The Cancer Proteome Atlas.

Table S3 KEGG enrichment analysis of mouse (mmu) proteins by anlotinib in A549 xenografts

Ontology	ID	Description	GeneRatio	BgRatio	pvalue	p.adjust	qvalue
Mmu (down)							
KEGG	mmu05132	Salmonella infection	23/262	253/8,910	1.39e-06	3.01e-04	2.18e-04
KEGG	mmu03040	Spliceosome	16/262	136/8,910	2.19e-06	3.01e-04	2.18e-04
KEGG	mmu05145	Toxoplasmosis	13/262	110/8,910	1.90e-05	0.002	0.001
KEGG	mmu05161	Hepatitis B	16/262	163/8,910	2.28e-05	0.002	0.001
KEGG	mmu05014	Amyotrophic lateral sclerosis	25/262	370/8,910	8.59e-05	0.005	0.003
Mmu (up)							
KEGG	mmu03013	RNA transport	17/253	182/8,910	1.54e-05	0.002	0.002
KEGG	mmu05014	Amyotrophic lateral sclerosis	26/253	370/8,910	1.72e-05	0.002	0.002
KEGG	mmu03040	Spliceosome	14/253	136/8,910	2.99e-05	0.003	0.003

KEGG, Kyoto Encyclopedia of Genes and Genomes.

https://dx.doi.org/10.21037/atm-22-5438